

The Relation between Luminous AGNs and Star Formation in Their Host Galaxies

Xu, Lei¹, Rieke, G. H.¹, Egami, E.¹, Haines, C. P.^{1,3}, Pereira, M. J.¹, & Smith, G. P.²

ABSTRACT

We study the relation of active galactic nuclei (AGNs) to star formation in their host galaxies. Our sample includes 205 Type-1 and 85 Type-2 AGNs, 162 detected with *Herschel*, from fields surrounding 30 galaxy clusters in the **Local Cluster Substructure Survey** (LoCuSS). The sample is identified by optical line widths and ratios after selection to be brighter than 1 mJy at $24\mu\text{m}$. We show that Type-2 AGN [OIII] λ 5007 line fluxes at high z can be contaminated by their host galaxies with typical spectrograph entrance apertures (but our sample is not compromised in this way). We use spectral energy distribution (SED) templates to decompose the galaxy SEDs and estimate star formation rates, AGN luminosities, and host galaxy stellar masses (described in an accompanying paper). The AGNs arise from massive black holes ($\sim 3 \times 10^8 M_\odot$) accreting at $\sim 10\%$ of the Eddington rate and residing in galaxies with stellar mass $> 3 \times 10^{10} M_\odot$; those detected with *Herschel* have IR luminosity from star formation in the range of $L_{\text{SF,IR}} \sim 10^{10} - 10^{12} L_\odot$. We find that: 1.) the specific star formation rates in the host galaxies are generally consistent with those of normal star-forming (main sequence) galaxies; 2.) there is a strong correlation between the luminosities from star formation and the AGN; and 3.) however, the correlation may not result from a causal connection, but could arise because the black hole mass (and hence AGN Eddington luminosity) and star formation are both correlated with the galaxy mass.

Subject headings: Galaxies: active–quasars: general–infrared: galaxies

1. Introduction

A key question in galaxy evolution is how the link is established and maintained between the mass of stars in a galaxy bulge and the mass of the super massive black hole (SMBH) in its center (e.g., Magorrian et al. 1998; Tremaine et al. 2002; Kormendy & Ho 2013). To probe this issue, we need to understand in detail the connection between accretion and star forming activity over cosmic time in AGNs and their hosts (Heckman & Best 2014).

¹ Steward Observatory, 933 N. Cherry Ave, University of Arizona, Tucson, AZ 85721, USA

² School of Physics and Astronomy, University of Birmingham, Edgbaston, Birmingham B15 2TT, UK

³ Departamento de Astronomia, Universidad de Chile, Casilla 36-D, Correo Central, Santiago, Chile

Because of the extreme luminosities of Type-1 AGN, they account for much of the accretion by SMBHs and therefore are critical to understanding this link. Their study has produced an overall understanding of the growth of mass in nuclear black holes (e.g., Marconi et al. (2004); Heckman & Best (2014)). The picture of star-forming galaxy evolution and of the growth of stellar mass at $z < 2$ is also becoming more clear. Star formation rates (SFRs) in normal star-forming galaxies are proportional to the galaxy stellar mass, with specific SFRs (SSFR, i.e., the star formation rate per unit stellar mass) increasing with redshift (e.g., Noeske et al. 2007; Elbaz et al. 2007; Daddi et al. 2007). Typical vigorously star-forming galaxies lie on a “main sequence”, where star formation is likely induced by internal processes such as turbulence and disk instabilities. However, a significant fraction of galaxies with stellar masses $\geq 3 \times 10^{10} M_{\odot}$ have SSFRs well below the main sequence, which therefore needs to be interpreted as an upper limiting case for the majority of star-forming galaxies. In addition, starbursting galaxies are a minority undergoing an episode of elevated star formation that places them well above the main sequence.

Despite these advances, studying the co-evolution of stellar and SMBH mass growth is challenging. Since the host galaxies are often hidden in the UV, optical, and NIR by the strong glare of the AGN, using these bands to compare the AGN host galaxy pattern of star formation with that in normal galaxies is very difficult. The mid-infrared aromatic (hereafter PAH) feature luminosity is found to be correlated to other possible SFR indicators in the quasar spectra, such as far infrared (FIR) luminosity. The PAH features in quasar and radio galaxy spectra at low- z (Schweitzer et al. 2006; Shi et al. 2007; Dicken et al. 2012; Shi et al. 2014), intermediate- z (Shi et al. 2009), and high- z (Maiolino et al. 2007; Lutz et al. 2008; Shipley et al. 2013) are direct evidence for star formation. Further evidence of star formation in AGN hosts comes from CO detection of quasars from low- z to high- z (e.g. Scoville et al. 2003, Solomon & Vanden Bout 2005, Wang et al. 2010). The CO line luminosities are also correlated with the FIR luminosities (e.g. Riechers et al. 2011). The correlations between FIR luminosity and these other star formation tracers suggest that FIR measurements may offer a useful approach for characterizing this process in the host galaxies.

Prior to *Herschel*, the measurements of rest-frame FIR emission from AGNs were limited to a small population (e.g., Omont et al. 2001; Haas et al. 2003; Dicken et al. 2008). With the advent of *Herschel*, it is possible to study the FIR properties efficiently for much larger samples. The sensitivity and wavelength coverage of *Herschel* (PACS: 100, 160 μm ; SPIRE: 250, 350, and 500 μm) can sample the IR spectral energy distributions (SEDs) of AGNs up to $z \sim 3$. A number of Type-1 AGN studies with *Herschel* have been reported. For example, Hatziminaoglou et al. (2010) present SPIRE data for a heterogeneously selected (from SDSS/MIR) Type-1 AGN sample at $z \sim 0 - 3$. The SPIRE 3-band colors of their *Herschel*-detected AGN are indistinguishable from those of non-AGN star-forming galaxies. Leipski et al. (2013) publish *Herschel* data for eleven 1.2 mm-selected Type 1 AGNs at $z \sim 6$, and show that five emit strongly in the FIR. Leipski et al. (2014) extend this survey to a total of 69 systems, of which $\sim 30\%$ are detected in the FIR. These studies find that an AGN-powered torus is not enough to account for all the FIR emission of *Herschel*-detected AGNs, and a star forming component is needed. *Herschel* observations have

also been reported for X-ray selected, moderate luminosity AGNs at $z \sim 0.5 - 3$ (e.g., Shao et al. 2010; Mullaney et al. 2012). Mullaney et al. (2012) find that the majority (79%) of their *Herschel*-detected AGNs reside in massive, normal star-forming galaxies, where the star formation appears to be induced by internal processes rather than by major mergers. However, no correlation is found between the X-ray luminosity from AGN and the FIR luminosity powered by star formation. Dicken et al. (2012) used *Spitzer* data on nearby radio galaxies to show that there is no connection between star formation in the hosts and the nuclear activity. Rosario et al. (2013) studied a relatively luminous quasar sample and found the mean SFRs of the host galaxies were consistent with the galaxy ‘main sequence’ and could be linked to the AGN properties through a common dependence on stellar mass. However, this study relies on stacking to complement the individual FIR detections, so their conclusions may not hold for a minority of galaxies with above-average SFRs. In addition, the stacking results may be influenced by far-infrared-quietest host galaxies. The presence of a significant quiescent host population seems likely, since local quasars can occupy quiescent hosts. For example, Shi et al. (2014) find that 16 of 84 PG quasars (or 19%) have SFRs $\leq 1 M_{\odot}/\text{yr}$.

In most previous work, the AGN sample was defined through optical spectroscopy (e.g., Hatziminaoglou et al. 2010, Rosario et al. 2013), or X-ray emission (e.g., Rafferty et al. 2011; Mullaney et al. 2012). Both of these metrics should emerge after obscuring circumnuclear material has cleared; that is, they represent late-phase AGNs, if we assume an evolution from gas inflow to activating an AGN to gas outflow (e.g., Hopkins 2012). Some previous studies are based on incomplete wavelength coverage with *Herschel* (e.g. only SPIRE, Hatziminaoglou et al. 2010; or only PACS, Rosario et al. 2013), thus limiting the accuracy with which the far infrared SEDs can be determined. In addition, virtually all of these works center on moderate-luminosity AGN (e.g., Shao et al. 2010; Mullaney et al. 2012; Rosario et al. 2013), which may be substantially below the SMBH Eddington luminosities and hence require modeling to relate the average (or peak) nuclear activity to host galaxy properties (e.g., Chen et al. 2013; Hickox et al. 2013). Finally, in many studies the sample of galaxies detected in at least two *Herschel* bands (supporting accurate SED fitting) is relatively small (e.g., 49 in Hatziminaoglou et al. 2010, 38 in Rosario et al. 2013). Consequently, the conclusions based on these previous works are sometimes inconclusive or contradictory.

We will augment and improve on these studies in a number of ways. The 205 Type-1 AGNs in our sample are uniformly selected from a 5.2 deg^2 survey area, on the basis of $24 \mu\text{m}$ flux density above 1 mJy. We complement these objects with 85 Type-2 AGN, selected in the same way from part of the same area. We draw 15 galaxies from this latter sample that are directly comparable with the Type-1 AGNs in terms of black hole masses and accretion rates, and which fall within the same redshift range. A multi-wavelength data set from the UV to FIR allows us to disentangle the SEDs into stellar, AGN, and star formation components, as described in an accompanying paper (Xu et al. 2015).

An important aspect of our study is the concentration on very luminous AGNs. The sample is selected on the basis of AGN luminosity at $24 \mu\text{m}$ (which dominates over star formation at this

wavelength for every object). This band is a rough indicator of AGN luminosity at the typical redshift of $z \sim 1$ (Spinoglio et al. 1995), so the Type-1 sample is complete for high luminosities (as a function of the appropriate redshift-dependent luminosity threshold). Most of the sources have black holes of mass $\geq 10^8 M_\odot$, accreting at 3% or more of the Eddington rate. Because the sources in our study are emitting close to the Eddington limit and hence uniformly represent approximately the maximum states of their outputs, our conclusions are not hostage to modeling the AGN variability. There have been a number of suggestions that Type 2 AGN may lie in galaxies with relatively high rates of star formation, made both from a theoretical perspective (Wada & Norman 2002; Ballantyne et al 2006) and from observations (e.g., Maiolino et al. 1995; Mouri & Taniguchi 2002; Buchanan et al. 2006; Deo et al. 2007; Meléndez et al. 2008; Baum et al. 2010; Castro et al. 2014; Villarroel & Korn 2014). This result is controversial (e.g. Pereira-Santaella et al 2010; Diamond-Stanic & Rieke 2012; Merloni et al. 2014); nonetheless, the Type-2 members of our sample test whether our conclusions are valid for such systems.

We find that there is substantial star formation in most of the AGN hosts. However, we also show that the AGNs at $z < 2$ reside in massive galaxies, and the majority of their hosts lie on or below the main sequence of normal star-forming galaxies. The high AGN and star forming luminosities need not have a direct causal connection, but may be linked through their mutual dependence on the masses of the host galaxies.

This paper is structured as follows. In Section 2 we summarize briefly the analyses of our sample in Xu et al. (2015). In Section 3 we analyze the star-forming properties of the AGN host galaxies and discuss how they might influence AGN selection approaches. Section 4 is used to derive the expected joint behavior of star formation and black hole accretion luminosity. We then compare this prediction with our results and with those in the literature. In Section 5 we compare our results with theoretical studies of the co-evolution of massive galaxies and their central black holes. Our conclusions are summarized in Section 6. Throughout this paper we assume $\Omega_M = 0.3$, $\Omega_\Lambda = 0.7$, and $H_0 = 70 \text{ km s}^{-1} \text{ Mpc}^{-1}$.

2. Prior Results

In Xu et al. (2015), we derived masses, black hole accretion rates, and star formation rates for the galaxies in this study. We also reached the following conclusions relevant to the following discussion:

1. About 50% (107 out of 205) of the Type-1 AGNs in our sample are individually detected by *Herschel*. Among these AGNs, 68% show high levels of star formation (the star formation activity contributes over 50% in the FIR). *Herschel* non-detected AGNs were studied using stacking analysis. On average, they have a similar level of AGN luminosity and similar optical colors, but the average star formation activity is several times lower compared with AGNs individually detected by *Herschel*.

2. Similarly, about 65% (55 out of 85) of the Type-2 AGNs are individually detected by *Herschel*. However, these objects tend to be at relatively low redshift and some of the 24 μm detections are a result of vigorous star formation, not just nuclear activity. We defined a High Luminosity Sample (HLS) and from it a Comparison Sample of 15 Type-2 AGN with properties (M_{BH} , Eddington ratio, and redshift) that make them directly analogous to the Type-1 sample.
3. The [OIII] λ 5007 emission line, commonly taken to be a measure of Type-2 AGN luminosity, does not show a 1:1 correspondence with this quantity in our data; instead, the line luminosity increases faster than the bolometric AGN luminosity.
4. The FIR-detected Type-1 AGNs and the 15 matching Type-2 ones reside in massive galaxies ($\sim 1 - 2 \times 10^{11} M_{\odot}$). They harbor supermassive black holes of $\sim 3 \times 10^8 M_{\odot}$, which accrete at $\sim 10\%$ of the Eddington luminosity.
5. The 24 μm -selected sample of Type-1 AGNs includes about twice as many objects as are identified through the Sloan Digital Sky Survey (SDSS), including the majority of the SDSS identifications. The additional objects have redder optical colors than typical SDSS quasars, due to reddening or intrinsically red quasar continua. There are also as many 24 μm -selected Type-1 AGNs as would be found in the X-ray in a survey to a similar bolometric luminosity limit. Therefore, our sample is representative of powerful Type-1 AGNs in general (and of Type-2 AGNs with similar black hole masses); the infrared selection has not biased the sample toward some minority of AGNs particularly detectable in the infrared.

We now build on the data and analysis in Xu et al. (2015) to investigate the underlying relationship of the AGNs to their host galaxies.

3. Host galaxy characteristics

3.1. Host galaxies lie on the main sequence

The specific star formation rates (SSFRs: star formation rate divided by stellar mass) for the Type-1 sample are shown in Figure 1. Those based on stellar masses determined by spectral deconvolution and the resulting estimate of the near-infrared stellar fluxes are shown as red filled circles. The values based on the indirect estimates of the galaxy stellar mass (based on the M_*/M_{\bullet} relation and the M_{\bullet} measurements for the Type-1 AGNs) are shown as blue filled squares. The lower open blue squares show one side of the rms scatter (Xu et al. 2015) in the relation for galaxies of the large masses typical of our sample¹. The upper open squares are a factor of four above the

¹The lower open squares also show the direct relation obtained by comparison of the K-band masses with those for the same galaxies from the M_*/M_{\bullet} relation. However, this value is anomalously low because the galaxies with stellar populations bright enough in the near infrared to outshine the AGNs and allow us to estimate M_* will be biased within the scatter to have relatively large values of M_*/M_{\bullet} .

nominal values to accommodate both the scatter and a possible selection bias — our very bright AGNs may have led us to host galaxies with relatively massive black holes within the scatter of the M_*/M_\bullet relation. See Xu et al. (2015) for further discussion.

As shown in Table 1, our full sample (Type-1 plus Type-2) consists of the maximally star-forming galaxies in very similar portions ($\sim 55\%$) independent of redshift. Figure 1 shows the massive galaxy main sequence (Elbaz et al. 2011), an upper limit of three times the MS SSFR (the rms scatter around the MS is 0.3 dex (Lutz 2014), so this limit is 1.6σ high). We have adopted a lower limit of 10% because of evidence of bimodality in the SSFR, with a dividing line between active and inactive galaxies about an order of magnitude below the main sequence (Wetzell et al. 2012). The maximally star-forming quasar host galaxies generally fall on the main sequence, with few galaxies outside these bounds. The remaining Type-1 AGN host galaxies will fall toward the bottom of the main sequence zone in Figure 1, as shown by the stacking results, or if there are quiescent hosts, below this zone (Wetzell et al. 2012).

The SSFRs of the Type-2 High Luminosity Sample (HLS) members as a function of redshift are shown in Figure 2 (along with similar results for the remainder of the Type-2 galaxies). The HLS members are indicated by squares, filled for the Comparison Sample, and the remaining galaxies are small dots. The SSFRs of most of the galaxies are consistent with those of the main sequence of normal star-forming galaxies, although some are at the upper bound of this range. The points for the Comparison Sample lie around the main sequence, showing that the members of the type-2 sample that most resemble the strongly-star-forming Type-1 sample similarly have main-sequence levels of star formation in their host galaxies.

There are a small number of galaxies in the combined Type-1 and Type-2 sample that are undergoing starbursts. The most noteworthy is J101805.93+385755.8, with a Type-2 AGN and a very strong component due to young, hot stars in our decomposition. Because its stellar output appears to be significantly influenced by young stars, the mass we have estimated is an upper limit, so its SSFR in the figure is shown as a lower limit. However, starbursts also appear among field galaxies (e.g. Elbaz et al. 2007), within the small-sample statistics at about the same rate as in the AGN hosts.

3.2. No strong dependence of host SSFRs on morphology

For the Type-2 host galaxies, the AGN is sufficiently faint in the optical that we were able to examine the galaxy morphologies (Xu et al. 2015). Figure 3 shows the IR star formation luminosity and SSFR as a function of redshift for different types of host galaxy. We do not find any correlation between the star formation and the morphological types. The five AGN hosts showing probable interaction do not have more star formation than the other types, as found for a much larger sample by Villforth et al. (2014) and Sabater et al. (2015), among others. All types of hosts form stars at rates consistent with normal star forming galaxies. However, our study of morphologies is limited

by the resolution of the images and the small sample size.

3.3. Use of [O III] as a AGN Luminosity Indicator

Xu et al. (2015) found a significant departure from the expected 1:1 relation between [O III] and bolometric AGN luminosity in the direction of an increasing [OIII] luminosity for more luminous AGN, an effect also reported by LaMassa et al. (2010), Hainline et al. (2013), and Shao et al. (2013) (in the latter case for only one of two infrared bands). Hainline et al. (2013) propose that the effect arises because of limitations on the extent of the narrow line region with increasing AGN luminosity. The fact that we have an independent estimate of the star formation in the host galaxy lets us identify an additional possible contributor. Conventional groundbased spectra (fiber diameters or slit widths of 1 - 2 arcsec) of galaxies at moderate to high redshift and with active nuclei might return [O III] measurements contaminated by star formation in the host galaxies. For example, our 1".5 fibers subtend 6.7 kpc at $z = 0.3$ and 10 kpc at $z = 0.6$. Since in typical AGN samples the most luminous members tend to be the most distant, this would yield an increase in [OIII] more rapidly than just in proportion to the AGN luminosity.

We can evaluate this possibility quantitatively. From the relations in Kennicutt (1998), the $H\beta$ luminosity in a star forming galaxy is about $0.2 \times A_{H\alpha-H\beta}\%$ of the infrared luminosity (assuming Case B and an extinction of $A_{H\alpha-H\beta}$ between $H\alpha$ and $H\beta$). From Moustakas & Kennicutt (2006), the [OIII] $\lambda 5007$ line is on average roughly the same intensity as $H\beta$ in the integrated light of star-forming galaxies. Therefore, assuming modest extinction, we can adopt $L([\text{OIII}])/L(\text{IR}) \sim 0.1\%$ for typical star-forming galaxies. From Diamond-Stanic et al. (2009) and Rigby et al. (2009) one finds that the luminosity of [OIII] $\lambda 5007$ is about 0.1% of the bolometric luminosity of a Type-2 AGN. This value is consistent with the 0.17% for the extinction-free [OIII] $\lambda 5007$ luminosity as adopted by Heckman & Best (2014). Comparing these values with the relative luminosities in Table 8 of Xu et al. (2015) indicates that there is indeed a possibility of contamination of the [OIII] line by emission due to star formation for spectrograph fibers that include a substantial part of the host galaxy. One might expect from this hypothesis that the ratio of [OIII] to $H\beta$ would tend to decrease with increasing redshift. Our data show a weak tendency in this direction, but the scatter is large and the result is not statistically significant; it should be tested in larger samples.

4. Connection between Star Formation and Active Nucleus Luminosity

We have just shown that the strongly star-forming, *Herschel*-detected, AGN hosts nearly all lie on the star-forming galaxy main sequence. Our stacking analysis indicates that the *Herschel*-non-detected galaxies lie in the lower part of the main sequence, although some could also lie below it (Xu et al. 2015). The morphology study is also consistent with this result – most of the AGNs in our sample are not interacting, and hence not interaction-induced starbursts. Even those that

are interacting do not have particularly high levels of star formation. These results indicate there is no obvious causal relation between nuclear activity and elevated star formation in a host galaxy; we probe this possibility in more depth in this section by examining the nature of the apparent connection between star formation and AGNs within individual galaxies.

4.1. The predicted $L_{\text{SFstrong}} \propto L_{\text{AGN}}$ relation

A general correlation between star formation rate, i.e. infrared luminosity, and AGN luminosity for quasars was found some time ago, (e.g., Lutz et al. (2008), Netzer(2009), Shao et al. (2010)). There have been suggestions that the correlation implies a causal connection between the two kinds of activity. To evaluate these suggestions, we first derive the connection between the star forming luminosity and that of the AGN assuming the AGN hosts are normal galaxies, forming stars sufficiently vigorously to place them on the main sequence. To distinguish them from galaxies at the lower part of the main sequence or that are quiescent, we designate them as having *Herschel* fluxes indicative of strong star formation. For the purpose of discussion the derivation that follows makes the assumption that their level of star formation is *not* necessarily affected by the presence of an AGN.

The output of a quasar powered by a black hole with mass M_{\bullet} is typically expressed in terms of the Eddington limit, i.e.,

$$L_{\text{AGN}} = \epsilon L_E = 3.2 \times 10^4 \epsilon \left(\frac{M_{\bullet}}{M_{\odot}} \right) L_{\odot}, \quad (1)$$

where ϵ (~ 0.1 for luminous AGNs) is the efficiency of converting gravitational potential energy to electromagnetic radiation. Conversely, Equation 1 can be used to estimate M_{\bullet} for a quasar near maximum output. The black hole mass is related to the stellar mass of the quasar host galaxy by $M_{*}/M_{\bullet} = \eta \sim 700$. The SFR for galaxies on the main sequence is

$$\text{SFR} = C_1 M_{*}^{\beta} \quad (2)$$

Various values of β have been derived, all consistent with 0.8. Elbaz et al. (2007) find $\beta = 0.9$ for their data and also show that the Millenium model gives $\beta = 0.8$; Noeske et al. (2007) derive $\beta = 0.7$; Tyler et al. (2013) find $\beta = 0.71$.

Equation 2 applies locally. Star formation in galaxies can be fitted by luminosity evolution as $(1+z)^{\alpha}$ with $\alpha \sim 3.2$ for $0 < z < 1$ (Rujopakarn et al. 2010), and with a smaller value of α at higher z . We also have Equation 3,

$$\frac{\text{SFR}}{M_{\odot} \text{ yr}^{-1}} = 1.2 \times 10^{-10} \left(\frac{L_{\text{SF,IR}}}{L_{\odot}} \right). \quad (3)$$

the classic relation between infrared luminosity (from 8 to 1000 μm) and the SFR (Kennicutt 1998)². Combining Equations 1, 2, 3, and the M_*/M_\bullet correlation, we get

$$L_{\text{SF}} = C_2(1+z)^\alpha \left(\frac{\eta L_{\text{AGN}}}{\epsilon} \right)^\beta. \quad (4)$$

This is consistent with Netzer’s result (2009) of $L_{\text{SF}} \propto L_{\text{AGN}}^{0.8}$. The quasar tracks in Lutz et al. (2008) and Shao et al. (2010) can also be fitted well by the correlation $L_{\text{SF}} \propto L_{\text{AGN}}^\beta$ with $\beta \sim 0.8$. Our derivation of Equation 4 shows that this relation can arise through the dependence of *both* the SFR *and* the mass of the SMBH on the mass of the host galaxy, without any other connection between the two activity types.

4.2. The observed correlation between AGN and SF luminosity

4.2.1. Approach

We now use our own sample to gain more understanding of the relation of AGN and star forming luminosities reflected in the diagrams of Lutz et al. (2008), Netzer(2009), and Shao et al. (2010). To compare with the prediction derived in the preceding section, we will determine the slope of the $L_{\text{SFstrong}} \propto L_{\text{AGN}}$ relation. We have added “strong” to the SF subscript as a reminder that we are not interested in the slope for all of the galaxies in the AGN sample, but only for those toward the upper range of star formation and hence that should fall on or above the galaxy main sequence.

The dependence of the detectable luminosity on z for our flux-limited sample might be expected to result in strong selection effects, leading to a slope that was influenced by the change in detection rate with *Herschel* as a function of redshift. Fortunately, this concern is unfounded. As shown in Table 1, the combination of the approximate proportionality of the SFR and AGN luminosity, plus the negative K-correction in the far infrared, have resulted in our overall sample (Type 1 plus Comparison Sample of Type 2 AGN) to be detected by *Herschel* at the same rate independent of redshift. Therefore, we can calculate the slope on the basis of the *Herschel*-detected galaxies knowing that they are in the upper 55th percentile of star formation irrespective of redshift.

Inclusion of galaxies with lower levels of far-IR emission could, in fact, bias the result because the undetected part of our sample may include quiescent host galaxies. For example, a proportion of $\sim 19\%$ quiescent galaxies, as found in the PG sample (e.g., Shi et al. 2014) would, if included in the slope calculation, make the overall slope flatter than if it were based only on the strongly star forming part of the sample. We have simulated this situation using a model with 81% of the simulated galaxies having SFRs strictly proportional to AGN luminosity and 19% with SFRs equal

²adjusted to our adopted IMF - see Xu et al. (2015)

to each other and independent of AGN luminosity. A linear fit (in log-log space) has a slope of 0.73. Thus, one might conclude despite a 1:1 relation between AGN luminosity and SFR for the strongly star forming galaxies, that the intrinsic relation was not 1:1. For this reason, we do not include the stacked results in fitting the behavior, nor do we use statistical methods to extend into the range where we do not have solid detections.

4.2.2. Results

In Figure 4 we combine the Type-1 sample and Type-2 Comparison Sample; the AGN and SF luminosities cover three and 2.5 orders of magnitude for the whole AGN sample, respectively. The best fit is $L_{\text{SF}} \propto L_{\text{AGN}}^{0.59}$. We have tested whether a simple linear regression is an adequate fit by fitting with polynomials of order 2, 3, and 4; none of them had any significant effect on the reduced χ^2 , so by Occam’s Razor the linear fit is preferred. The Jarque-Bera test indicates that the residuals from the linear fit are normally distributed ($p = 85.1\%$), in agreement with the Shapiro-Wilk Test ($p = 39.2\%$). A fit to the residuals indicates a rms scatter of ~ 0.4 dex, which is consistent with expectations from the scatter of ~ 0.3 dex for purely star forming galaxies around the main sequence (Brinchmann et al. 2004; Lutz 2014) with a modest increase due to the expected scatter in Eddington ratios. Various alternative samples, e.g. discarding galaxies where the warm component fit could account for significant fraction of the far infrared luminosity, do not change the slope significantly.

We now consider whether we can rule out the hypothesis that the star formation in the host galaxies has a 1:1 correlation with the AGN luminosity, as might be expected if they are linked causally. To do so, we use the $\Delta\chi^2$ method (Press et al. 2002) to evaluate the range of slopes that can fit the data in Figure 4. Because the errors on the luminosities are not known *a priori*, we set them to be equal and to a value so the reduced $\chi^2 = 1$ for the best fit. We then computed χ^2 for other slopes and derived the corresponding probability that this parameter could be as large or larger than the computed value by chance. The result is that slopes of 0.7 are consistent with our measurements at $\sim 37\%$ probability, slopes of 0.8 at $\sim 15\%$, slopes of 0.9 at $\sim 1.7\%$ probability, and slopes of 1.0 are consistent only at the $\sim 0.02\%$ level. That is, the observations do not appear to support the expectation of a 1:1 correlation if there were a causal connection star forming and nuclear activity, but instead suggest that the observed relation could arise only due to their mutual dependence on galaxy mass.

As shown in Figure 4, there is a strong trend of increasing luminosity with redshift as a natural consequence of using a pencil beam survey to select the sample, so the relative volume in the survey increases rapidly with increasing redshift. However, this could also mean that the trends of star formation and AGN activity are dependent on evolution in ways not included in the analysis above. There are two obvious possibilities. First, the SMBHs of the particular maximally luminous AGNs in our study might grow substantially between $z \sim 2$ and $z \sim 0.5$ (although on average it is believed that the growth of the most massive black holes is nearly complete by $z = 2$ (e.g., Marconi et al.

2004; Trakhtenbrot & Netzer 2012)). In this case, the Eddington limits will go up and the most luminous AGNs will be more luminous locally, moving the low redshift/low luminosity points in Figure 4 to the right. The second is that the main sequence level of specific star formation decreases as we approach the current epoch, by about a factor of 3-4 between $z \sim 1.5$ and 0.5 (Elbaz et al. 2011). This behavior would move the low redshift/low luminosity points in Figure 4 down. Both effects would therefore make the observed slope steeper than it would be without these potential types of evolution. That is, the fitted slope is an upper limit at least so far as these two first-order evolutionary terms are concerned. Although this does not rule out the possibility of other, more complex changes affecting the slope, the existing evidence strongly suggests that the 1:1 relation does not hold.

As a final test, we have analyzed the behavior of the Eddington Ratio vs. the SSFR (using only values of the SSFR based on the photometric mass determinations). Since these quantities are normalized to remove slopes to first order, this comparison should show no dependence if there is no link between the quantities. We find that the slope of the relation is equal to 0.02 ± 0.30 . The large uncertainty arises because of the limited range of the Eddington ratios and the large scatter of both quantities.

4.3. Previous Studies of the Connection between AGN and SF

4.3.1. The Relation between SF and AGN Luminosities

There are several previous studies of the relation between AGN and SF luminosities. A strong correlation, $L_{\text{SFstrong}} \propto L_{\text{AGN}}^{0.8}$, has been demonstrated over more than five orders of magnitude in luminosity (Netzer 2009). The sample included PG quasars at $z \sim 0.1$ (Schweitzer et al. 2006), AGN-dominated Type-2 galaxies at low redshift ($z < 0.25$) identified using SDSS spectra, and strong submillimeter quasars at $z \sim 2 - 3$ (Lutz et al. 2008). These studies use different SF and AGN indicators for different types of AGN/host galaxy sources, and use data from surveys with different depths. Nonetheless, a correlation between AGN and SF luminosities was found for the luminous AGN systems within the whole sample. This study led to suggestions of direct links between black hole and bulge growth, at least for relatively luminous AGN. The most luminous AGNs in these studies should be similar to our AGN sample (either Type 1 or Type 2), i.e., accreting at $\sim 10\%$ of Eddington. However, as noted in the preceding section, the coefficient in this correlation is in good agreement with the value expected if the correlation arises only because of the mutual dependence of the rate of star formation and of M_{\bullet} on galaxy mass.

For X-ray-selected, low or moderate luminosity AGNs at $z \sim 0-3$, there is no strong correlation between AGN and SF luminosities for individually detected AGNs (e.g., Shao et al. 2010; Rosario et al. 2012; Mullaney et al. 2012; Rosario et al. 2013), even though these AGN host galaxies lie on the galaxy main sequence (Mullaney et al. 2012). One possible reason is that low or moderate luminosity AGNs have a large scatter in the distribution of Eddington ratios (e.g., Lusso et al.

2012). This scatter will also affect the correlation between AGN and SF luminosities. A simple model of the scatter in L_X due to AGN variability indicates that the correlation also exists for low and moderate luminosity AGNs (e.g. Chen et al. 2013; Hickox et al. 2013).

The correlation may be more evident for higher luminosity AGNs. Rafferty et al. (2011) studied the far infrared properties of AGNs in fields with very deep X-ray survey data, finding a strong correlation between star-forming luminosity and the presence of powerful AGNs. However, they point out that this effect could arise through the mutual dependence of both phenomena on stellar mass. Rosario et al. (2012) worked with a sample of X-ray selected AGNs using PACS data to study the correlation between L_{SF} and L_{AGN} . They found a strong correlation between $L_{60\mu\text{m}}$ and L_{AGN} for high luminosity AGNs ($L_{\text{AGN}} \sim 10^{44} - 10^{46}$ ergs s $^{-1}$) at $z < 1$, but not at high redshift ($z > 1$) (but with a very small subsample, only 4 objects). They claimed the reason for this trend is that at $z < 1$ major-mergers play important roles at the high luminosity end of both AGN and star formation activities, and the importance of major-mergers decreases at $z > 1$. However, assuming the Type-2 AGNs are representative of the $z < 1$ category, we find few examples of mergers, contrary to their prediction. Our result agrees with those from much larger samples (Villforth et al. 2014; Sabater et al. 2015).

Rovilos et al. (2012) report that a sample of X-ray selected AGNs have elevated SSFRs. In their Figure 9, 8 out of 13 X-ray quasars with intrinsic $L_{2-10 \text{ keV}} > 10^{44}$ ergs s $^{-1}$ at $z < 2$ are above the galaxy main sequence, and only 5 are on the galaxy main sequence or reside in quiescent galaxies. However, they may use the wrong AGN templates to decompose the SEDs. By matching the X-ray AGN source catalog for the CDFS, we are able to identify two sources at $z = 1.031$ and $z = 1.216$ in Fig 2 of Rovilos et al. (2012). The hardness ratios of these two sources are -0.16 and 0.45, respectively, using the data from the Chandra 2Ms survey catalog (Luo et al. 2008). This puts the first source in the unobscured AGN (Compton thin) category. The second is in a transitional region, but it has also been found to be Compton-thin (Tozzi et al. 2006). Therefore, the sources should not be fitted with an obscured template as was done by Rovilos et al. (2012). In particular, a Type-1 AGN template should be used to fit the UV emission rather than a UV-bright galaxy template. Therefore the stellar masses, and hence the specific SFRs of these two X-ray quasars are not reliable. In general, fitting the UV with a young stellar population to compensate for the lack of UV output from the absorbed AGN template will significantly underestimate the stellar mass and overestimate the SSFR.

4.3.2. *The Coincidence of Star Forming and Nuclear Activity in the Same Galaxy*

Although we have argued that there is no compelling evidence for a causal link between elevated star formation and nuclear activity, a possible counter-example is provided by Symeonidis et al. (2013). They studied a sample of IR-luminous galaxies (detected at $70 \mu\text{m}$), X-ray detected Type 2 AGNs, and hybrid AGN/SF sources from COSMOS. They found that the IR luminous/star-forming galaxies and Type 2 AGN hosts have a significant overlap in color-magnitude space ($U - V/M_V$)

and color-color space ($U - V/V - J$), thus minimizing selection effects between the samples. They calculated the predicted numbers of hybrid AGN/SF sources in 0.5 magnitude bins of M_V and 0.25 magnitude bins in $U - V$ and $V - J$ assuming that the presence of an AGN and the star formation-powered IR emission in a given galaxy are independent events. They found that the predicted numbers of hybrid AGN/SF sources under this assumption are two-four times lower than the observed numbers; the discrepancy is removed if the two activities are not completely independent. They interpret this behavior as evidence for a causal link between black hole accretion and star formation.

The approach of Symeonidis et al. (2013) depends on there being no underlying selection bias that might favor *both* high rates of star formation *and* luminous nuclear activity. Since the detection rates in Symeonidis et al. (2013) are low ($\sim 0.6\%$ for infrared-emitters and $\sim 0.3\%$ for AGN), the detected galaxies are at the extreme high end of the luminosity distributions and any biases can have a strong effect that might mimic a causal connection. Both AGN and star forming luminosities have a dependence on host galaxy stellar mass. Star formation rates generally go as the 0.8 power of the mass (as already discussed). Although this value is strictly for the slope of the main sequence, the envelope for the star formation rates in galaxies above the main sequence has a similar slope (e.g. Wuyts et al. (2011), Figure 1, central panel) and in any case the most luminous infrared galaxies, which will be favored for detection in Symeonidis et al. (2013), tend to be very massive (Rothberg et al. 2013) and hence at the extreme high tail of the star formation rate distribution. For an AGN, the SMBH mass, and hence the Eddington Luminosity, is correlated with the stellar mass in the bulge. The most luminous AGNs will tend to have the highest Eddington Luminosities and thus massive galaxies are favored for detection.

These mass dependencies undermine the independence of high AGN and star-forming luminosities. The sample selected by Symeonidis et al. (2013) on the basis of color-color behavior does not control directly for mass and hence is particularly susceptible to this issue. We therefore examine in more depth their other selection approach, on the basis of $U - V$ and M_V . Although the host galaxy masses correlate with galaxy optical properties, e.g. M_V , the correlation between V -band magnitude and the stellar mass has a large scatter, of order a factor of 10 in a $\Delta M_V \sim 0.5$ magnitude bin (e.g., Shapley et al. 2001; Savaglio et al. 2005; Kannappan et al. 2007). Therefore, it is possible that the apparent correlation of AGN and $70 \mu\text{m}$ sources is influenced by their dependence on mass even in a sample selected in 0.5 magnitude bins of M_V .

We ran a simple simulation to test this possibility. In each bin of M_V , within a bin size of 0.5 mag, say $[M_{V,0}, M_{V,0} + 0.5]$, we assume the mass to be evenly distributed in the range of $[1M_{*,0}, 10M_{*,0}]$. Specifically, we distribute the mass over 10 small bins in this range to compare with the case where M_V is a perfect mass indicator and predicts host stellar mass tightly correlated with M_V , $[4M_{*,0}, 5M_{*,0}]$. We use the SFR probability distribution around the main sequence from Brinchmann et al. (2004) to estimate the probability distribution of the IR emission as a function of host galaxy stellar mass; this distribution includes starbursting galaxies that might dominate the far infrared detections. For luminous AGNs, we assume the Eddington ratio probability distribution

follows the G-model in Shankar et al. (2013).³ For each given galaxy stellar mass, we estimate the black hole mass using the M_*/M_\bullet relation. Then we convert the Eddington ratio probability distribution to an AGN luminosity probability distribution.

We use these two distributions of IR and AGN luminosity at a given mass to estimate the probability that the IR or AGN luminosity will fall above the selection threshold for the cases: 1.) where the stellar masses all lie within a narrow range; or 2.) where the stellar masses are spread over a range of a factor of ten. The results for the case of AGNs are shown in Figure 5; those for IR luminosity are very similar. We found that Case 2 has a much larger probability that the IR or AGN luminosity falls above the detection/selection threshold, and that the increased detection rate is largely due to the most massive galaxies in the assumed mass range. For example, M_V in the range of [-20.5, -21] magnitude corresponds (with mass errors) to a range of $4 \times 10^9 - 4 \times 10^{10} M_\odot$. If the stellar masses are all in the center of this range, the probability of sources with AGN X-ray luminosity above $6 \times 10^{42} \text{ ergs s}^{-1}$ is 0.3%, as in Symeonidis et al. (2013) (M. Symeonidis, private communication). This value is also typical of the detection rates in their full sample. If the stellar masses spread out over the 10-times larger range, the probability of the sources of this M_V with AGN X-ray luminosity above $6 \times 10^{42} \text{ ergs s}^{-1}$ is six times higher. We obtain a similar result for IR luminosities.

Our conclusion is that the galaxy stellar masses strongly affect the detection rates for SFR at 70 μm and for AGN. This behavior will reproduce the tendency for the two phenomena to occur together, as observed by Symeonidis et al. (2013), from which they inferred a causal connection between star formation and nuclear activity. However, in our simulation, the behavior arises purely because both phenomena have a strong mass dependence; there may be no need to hypothesize any additional causal connection.

5. Implications of not finding a direct link between AGNs and star formation in their host galaxies

5.1. Possible lack of a connection between star formation and black hole accretion

We have shown that the AGN host galaxies have normal, main-sequence levels of star formation. Although high levels of star formation and high AGN luminosities tend to occur together, the luminosities from these two phenomena do not correlate 1:1 as might be expected if there were a causal relation between the two activity types. One possible conclusion is that there is, in fact, no connection within the range of cosmic epochs probed in this study. However, if the SFR and AGN were completely decoupled, then there might be too much scatter in the M_*/M_\bullet relation, even if their growth somehow averaged out over time. One proposal is that the correlation is a result of the

³a Gaussian in $\log \lambda_c$ with dispersion of 0.3 dex, and centered at $\log \lambda_c = -0.6$.

process of hierarchical assembly in a Λ CDM Universe through the Central Limit Theorem (Peng 2007; Jahnke & Macciò 2011), i.e., the link is causal but was established early in the assembly of these galaxies.

5.2. Is black hole accretion delayed relative to star formation?

Another possibility is that any correlation is not simultaneous, but the AGN activity is delayed. The timescales of the starbursts in ULIRGs are estimated to be short, that is no more than 10^7 to 10^8 years in the most luminous systems, and perhaps in some cases as small as $5 - 10 \times 10^6$ years (Genzel et al. 1998, Thornley et al. 2000). These short timescales are in agreement with theoretical models (e.g., Chakrabarti et al. 2008; Hopkins et al. 2008; Cen 2012; Hopkins et al. 2013; Hayward et al. 2013). The models for AGN luminosity show similarly short peaks, but there is a range of predictions on when they occur relative to the peak of the star formation. Bekki et al. (2006) model the two phases to be nearly simultaneous. Hopkins et al. (2008) and Hopkins (2012) predict a delay of order 80 Myr for the peak of AGN luminosity, but with a substantial overlap when both the AGN and starburst are very luminous. Cen (2012) argues for a longer delay, with the peak of AGN activity after the prime starburst has died out. There is already some observational evidence that the primary host galaxy star formation may occur up to 10^9 years before the peak AGN luminosity (Wild et al. 2007).

Our sample of AGN is selected in the mid-IR and hence is optimized for the early, blow-out, infrared-luminous phase in quasar development (e.g., Hopkins et al. 2008; Georgakakis et al. 2009; Glikman et al. 2012). Thus, any delays between the peak of star formation and the peak of AGN infrared luminosity should be minimized compared to the delays for AGN total luminosity or X-ray luminosity, for example. Nonetheless, we find little evidence for simultaneity in elevated star formation and near-Eddington AGN activity. This result would favor models with relatively long delays, such those of Wild et al. (2010) and Cen (2012).

6. Summary

We studied the properties of a $24 \mu\text{m}$ -selected spectroscopically-identified AGN sample using a multi-wavelength dataset from *GALEX*, SDSS, UKIRT, WISE, *Spitzer*/MIPS, and *Herschel*. We summarize the results from this study (including results from the accompanying paper by Xu et al. (2015)) as follows.

1. As also found, e.g., by Hainline et al. (2013), the strength of the [OIII] λ 5007 line increases more rapidly than proportionately to bolometric AGN luminosity (Xu et al. 2015). At relatively high redshift (and hence high AGN luminosity), detection of [OIII] emission from parts of the host galaxy within the spectrograph fiber may contribute to this effect.

2. A warm excess in the MIR was found for eight Type-1 AGNs compared with a local quasar template (Xu et al. 2015). This warm excess is more prominent at higher redshifts within our sample. It is not clear whether this change is due to evolution, or whether the warm excess is confined to very luminous quasars.
3. For $z > 0.3$, selection at $24 \mu\text{m}$ yields a sample of highly luminous Type 2 AGN (Xu et al. 2015). At lower redshifts, the sample is significantly contaminated by star forming galaxies.
4. For $0.3 < z < 0.8$ the numbers of luminous Type 1 and Type 2 AGN are similar (Xu et al. (2015)).
5. The host galaxies of luminous Type-1 and Type-2 AGNs have SSFRs consistent with the galaxy main sequence trend, i.e. they are normal, star forming galaxies.
6. There is a strong correlation between the IR luminosity of the star formation component and the AGN total luminosities.
7. However, the correlation differs significantly from the 1:1 correspondence that might be expected if the star formation and AGNs were related directly, and it could arise just because the BH mass (and hence Eddington limit) and the star formation are both correlated with the galaxy mass, rather than requiring a causal connection between the star formation and the nuclear activity.
8. Although a number of evolutionary models indicate that peaks of star formation and nuclear activity should occur closely in time, our results either indicate no connection in the two forms of activity over the cosmic epochs probed by our sample ($0.5 < z < 2$), or favor models where fueling of an AGN is well removed in time from the triggering of elevated star formation in the host galaxy.

7. Acknowledgements

We thank Xiaohui Fan, Desika Narayanan, and Dan Stark for helpful discussions. Jacopo Fritz provided AGN SED templates. We also thank Yong Shi for communicating results on quasar aromatic band measurements in advance of publication. This work is based in part on observations made with *Herschel*, a European Space Agency Cornerstone Mission with significant participation by NASA. Additional observations were obtained with *Spitzer*, operated by JPL/Caltech. We acknowledge NASA funding for this project through an award for research with *Herschel* issued by JPL/Caltech. CPH was funded by CONICYT Anillo project ACT-1122. GPS acknowledges support from the Royal Society. Additional support was provided through contract 1255094 from JPL/Caltech to the University of Arizona. This paper also is based in part on work supported by the National Science Foundation under Grant No. 1211349.

Funding for the SDSS and SDSS-II has been provided by the Alfred P. Sloan Foundation, the Participating Institutions, the National Science Foundation, the U.S. Department of Energy, the National Aeronautics and Space Administration, the Japanese Monbukagakusho, the Max Planck Society, and the Higher Education Funding Council for England. The SDSS Web Site is <http://www.sdss.org/>.

The SDSS is managed by the Astrophysical Research Consortium for the Participating Institutions. The Participating Institutions are the American Museum of Natural History, Astrophysical Institute Potsdam, University of Basel, University of Cambridge, Case Western Reserve University, University of Chicago, Drexel University, Fermilab, the Institute for Advanced Study, the Japan Participation Group, Johns Hopkins University, the Joint Institute for Nuclear Astrophysics, the Kavli Institute for Particle Astrophysics and Cosmology, the Korean Scientist Group, the Chinese Academy of Sciences (LAMOST), Los Alamos National Laboratory, the Max-Planck-Institute for Astronomy (MPIA), the Max-Planck-Institute for Astrophysics (MPA), New Mexico State University, Ohio State University, University of Pittsburgh, University of Portsmouth, Princeton University, the United States Naval Observatory, and the University of Washington.

This publication makes use of data products from the Wide-field Infrared Survey Explorer, which is a joint project of the University of California, Los Angeles, and the Jet Propulsion Laboratory/California Institute of Technology, funded by the National Aeronautics and Space Administration.

REFERENCES

- Ballantyne, D. R., Everett, J. E., & Murray, N. 2006, *ApJ*, 639, 740
- Baum, S. A., Gallimore, J. F., O’Dea, C. P. et al. 2010, *ApJ*, 710, 289
- Bekki, K., Shioya, Y., & Whiting M. 2006, *MNRAS*, 371, 805
- Brinchmann, J., Avelino, P., Martins, C., et al. 2004, *MNRAS*, 351, 1151
- Buchanan, C. L., Gallimore, J. F., ODea, C. P., Baum, S. A., Axon, D. J. et al. 2006, *AJ*, 132, 401
- Castro, A., Miyaji, T., Shirahata, M. et al. 2014, *PASJ*, 66, 110
- Cen, Renyue 2012, *ApJ*, 755, 28
- Chakrabarti, S., Fenner, Y., Cox, T. J., Hernquist, L., & Whitney, B. A. 2008, *ApJ*, 688, 972
- Chen, C.-T., Hickox, R. C., Alberts, S. et al. 2013, *ApJ*, 773, 3
- Daddi, E., Dickinson, M., Morrison, G. et al. 2007, *ApJ*, 670, 156
- Deo, R. P., Crenshaw, D. M., Kraemer, S. B., Dietrich, M., Elitzur, M. et al. 2007, *ApJ*, 671, 124
- Diamond-Stanic, A. M., Rieke, G. H., and Rigby, J. R. 2009, *ApJ*, 698, 623
- Diamond-Stanic, A. M., & Rieke, G. H. 2012, *ApJ*, 746, 168
- Dicken, D., Tadhunter, C., Morganti, R., Buchanan, C., Oosterloo, T., & Axon, D. 2008, *ApJ*, 678, 712
- Dicken, D., Tadhunter, C., Axon, D., Morganti, R., et al. 2012, *ApJ*, 745, 172
- Elbaz, D., Daddi, E., LeBorgne, D. et al. 2007, *A&A*, 468, 33
- Elbaz, D., Dickinson, M., Hwang, H. S. et al. 2011, *A&A*, 533, 119
- Genzel, R. Lutz, D., Sturm, E. et al. 1998, *ApJ*, 498, 579
- Georgakakis, A., Clements, D. L., Bendo, G., Rowan-Robinson, M., Nandra, K., & Brotherton, M. S. 2009, *MNRAS*, 394, 533
- Glikman, Eilat, Urrutia, T., Lacy, M. et al. 2012, *ApJ*, 757, 51
- Haas, M., Klaas, U., Müller, S. A. H. et al. 2003, *A&A*, 402, 87
- Hainline, K. N., Hickox, R., Greene, J. E., Myers, A. D., & Zakamska, N. L. 2013, *ApJ*, 774, 145
- Hatziminaoglou, E., Omont, A., Stevens, J. A. et al. 2010, *A&A*, 518L, 33

- Hayward, C. C., Torrey, P., Springel, V., Hernquist, L., & Vogelsberger, M. 2014, MNRAS, 442, 1992
- Heckman, T. M., & Best, P. M. 2014, ARA&A, 52, 589
- Hickox, R. C., Mullaney, J. R., Alexander, D. M. et al. 2014, ApJ, 782, 9
- Hopkins, P. F., Hernquist, L., Cox, T. J., & Keres, D. 2008, ApJS, 175, 356
- Hopkins, P. F. 2012 MNRAS 420, 8
- Hopkins, P. F., Cox, T. J., Hernquist, L., Narayanan, D., Hayward, C. C., & Murray, N. 2013, MNRAS, 430, 1901
- Jahnke, K. & Macciò, A. V. 2011, ApJ, 734, 92
- Kannappan, S. J., & Gawiser, E. 2007, ApJL, 657, 5
- Kennicutt, Jr., R. C. 1998, ARA&A, 36, 189
- Kormendy, John, and Ho, Luis C. 2013, ARA&A, 51, 511
- LaMassa, S. M., Heckman, T. M., Ptak, A., Martins, L., Wild, V., & Sonnentrucker, P. 2010, ApJ, 720, 786
- Leipski, C., Meisenheimer, K., Walter, F. et al. 2013, ApJ, 772, 103
- Leipski, C., Meisenheimer, K., Walter, F. et al. 2014, ApJ, 785, 154
- Luo, B., Bauer, F. E., Brandt, W. N. et al. 2008, ApJS, 179, 19
- Lusso, E., Comastri, A., Simmons, B. D. et al. 2012, MNRAS, 426, 623
- Lutz, D., Sturm, E., Tacconi, L. J. et al. 2008, ApJ, 684, 853
- Lutz, D. 2014, ARA&A, 52, 373
- Magorrian, J., Tremaine, S., Richstone, D. et al. 1998, AJ, 115, 2285
- Maiolino, R., Ruiz, M., Rieke, G. H., & Keller, L. D. 1995, ApJ, 446, 561
- Maiolino, R., Shemmer, O., Imanishi, M. et al. 2007, A&A, 468, 979
- Marconi, A., et al. 2004, MNRAS, 351, 169
- Meléndez, M., Kraemer, S. B., Schmitt, H. R., Crenshaw, D. M., Deo, R. P., Mushotzky, R. F., & Bruhweiler, F. C. 2008, ApJ, 689, 95
- Merloni, A., Bongiorno, A., Brusa, M. et al. 2014, MNRAS, 437, 3550

- Mouri, H., & Taniguchi, Y 2002, ApJ, 565, 786
- Mullaney, J. R., Pannella, M., Daddi, E. et al. 2012, MNRAS, 419, 95
- Netzer, H. 2009, MNRAS, 399, 1907
- Noeske, K. G., Weiner, B. J., Faber, S.J. et al. 2007, ApJL, 660, 43
- Omont, A., Cox, P., Bertoldi, F., McMahan, R. G., Carilli, C. L., and Isaak, K. G. 2001, A&A, 374, 371
- Peng, C. Y. 2007, ApJ, 671, 1098
- Pereira-Santaella, M., Diamond-Stanic, A. M., Alonso-Herrero, A., & Rieke, G. H. 2010, ApJ, 725, 2270
- Press, W. H., Teukolsky, S. A., Vetterling, W. T., & Flannery, B. P. 2002, "Numerical Recipes in C," 2nd Edition, Cambridge: Cambridge University Press
- Rafferty, D. A., Brandt, W. N., Alexander, D. M., Xue, Y. Q., Bauer, F. e., Lehmer, B. D., Luo, B., & Papovich, C. 2011, ApJ, 742, 3
- Riechers, D. A., Hodge, J., Walter, F., Carilli, C. L., and Bertoldi, F. 2011, ApJL, 739, 31
- Rigby, J. R. Diamond-Stanic, A. M., and Aniano, G. 2009, ApJ, 700, 1878
- Rosario, D. J., Santini, P., Lutz, D. et al. 2012, A&A, 545, 45
- Rosario, D. J., Trakhtenbrot, B., Lutz, D. et al. 2013, A&A, 560, 72
- Rothberg, B., Fischer, J., Rodrigues, M., & Sanders, D. G. 2013, ApJ, 767, 72
- Rovilos, E., et al. 2012, A&A, 546, 58
- Rujopakarn, W., Eisenstein, D. J., Rieke, G. H. et al. 2010, ApJ, 718, 1171
- Sabater, J., Best, P. N., & Heckman, T. M. 2015, MNRAS, 447, 110
- Savaglio, S., Glazebrook, K., Le Borgne, D. et al. 2005, ApJ, 635, 260
- Schweitzer, M., Lutz, D., Sturm, E. et al. 2006, ApJ, 649, 79
- Scoville, N. Z., Frayer, D. T., Schinnerer, E., and Christopher, M. 2003, ApJL, 585, 105
- Shao, L., Lutz, D., Nordon, R. et al. 2010, A&A, 518L, 26
- Shao, L., Kauffmann, G., Li, C., Wang, J., & Heckman, T. M. 2013, MNRAS, 436, 3451
- Shankar, F., Weinberg, D., & Miralda-Escude, J. 2013, MNRAS, 428, 421

- Shapley, A. E., Steidel, C. C., Adelberger, K. L., Dickinson, M., Giavalisco, M., & Pettini, M. 2001, *ApJ*, 562, 95
- Shi, Yong, Ogle, P., Rieke, G. H. et al. 2007, *ApJ*, 669, 841
- Shi, Yong, Rieke, G. H., Ogle, P., Jiang, Linhua, and Diamond-Stanic, A. M. 2009, *ApJ*, 703, 1107
- Shi, Yong, Rieke, G. H., Ogle, P. M., Su, K. Y. L., and Balog, Z. 2014, *ApJS*, 214, 23
- Shiple, H., Papovich, C., Rieke, G. H., Dey, A., Jannuzi, B. T., Moustakas, J., & Weiner, B. 2013, *ApJ*, 769, 75
- Solomon, P. M., and Vanden Bout, P. A. 2005, *ARA&A*, 43, 677
- Spinoglio, L., Malkan, M. A., Rush, B., Carrasco, L., & Recillas-Cruz, E. 1995, *ApJ*, 453, 616
- Symeonidis, M., Kartaltepe, J., Salvato, M. et al. 2013, *MNRAS*, 433, 1015
- Thornley, M. D., Forster-Schreiber, N. M.,utz, D., Genzel, R., Spoon, H. W., Kune, D., & Sternberg, A. 2000, *ApJ*, 539, 641
- Th
- Tozzi, P., Gilli, R., Mainieri, V. et al. 2006, *A&A*, 451, 457
- Trakhtenbrot, B., & Netzer, H. 2012, *MNRAS*, 427, 3081
- Tremaine, S., Gebhardt, K., Bender, R. et al. 2002, *ApJ*, 574, 740
- Tyler, K. D., Rieke, G. H., & Bai, L. 2013, *ApJ*, 773, 86
- Villforth, C., Hamann, F., Rosario, D. J. et al. 2014, *MNRAS*, 439, 3342
- Villarroel, B., & Korn, A. 2014, *Nature Physics*, 10, 417
- Wada, K., & Norman, C. A. 2002, *ApJ*, 566, L21
- Wang, Ran, Carilli, C. L., Neri, R. et al. 2010, *ApJ*, 714, 699
- Wetzell, A. R., Tinker, J. L., & Conroy, C. 2012, *MNRAS*, 424, 232
- Wild, V., Kauffmann, G., Heckman, T. et al. 2007, *MNRAS*, 381, 543
- Wild, V., Heckman, T., & Charlot, Stéphane 2010, *MNRAS*, 405, 933
- Wuyts, S., Forster-Schreiber, N.M., van der Wel, A. et al. 2011, *ApJ*, 742, 96
- Xu, Lei, Rieke, G. H., Egami, E., Pereira, M. J., Haines, C. P., & Smith, G. P. 2014, Submitted to *ApJS*

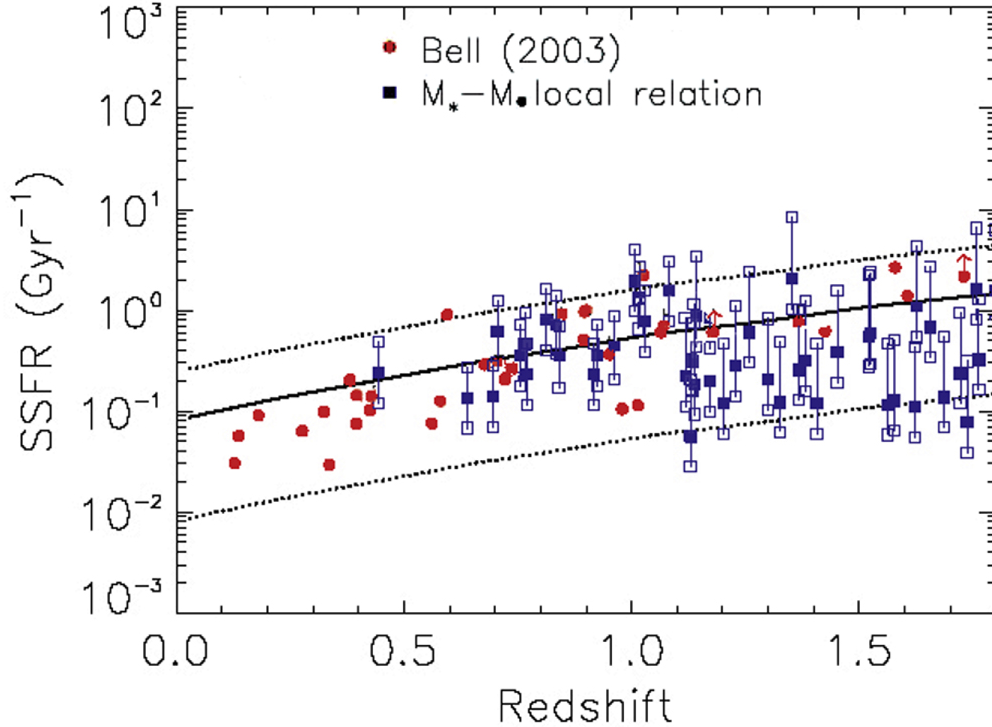


Fig. 1.— SSFR versus z for *Herschel*-detected Type-1 AGNs. The solid line is the SSFR of main sequence galaxies (Elbaz, et al. 2011). The dotted lines are a factor of three above or 10 below the SSFR of main sequence galaxies, respectively. The filled red circles represent sources with stellar mass estimated by K-band luminosity. The filled blue squares are represent sources with stellar mass estimated from the local mass ratio $M_*/M_\bullet = 700$. The lower open squares are the SSFR values using masses a factor of two lower than the local mass ratio, representing the $1\text{-}\sigma$ scatter in the M_*/M_\bullet relation. The upper open squares are show the upper rms scatter for $z < 1.1$ but above that value are a factor of four above the nominal estimates, allowing for an additional possible factor of two systematic error in the M_* estimates due to possible evolution and/or selection of the galaxies on the basis of exceptionally luminous AGNs

Table 1. Fraction of Herschel Detections in Full Sample

	total	$0 \leq z < 0.5$	$0.3 \leq z < 0.5$	$0.5 \leq z < 1$	$1 \leq z < 1.5$	$1.5 \leq z < 3$
<i>Herschel</i> -detected	157	55	24	38	29	35
total	285	96	51	76	54	59
fraction detected	0.55	0.57 ± 0.08	0.47 ± 0.10	0.50 ± 0.08	0.54 ± 0.10	0.59 ± 0.10

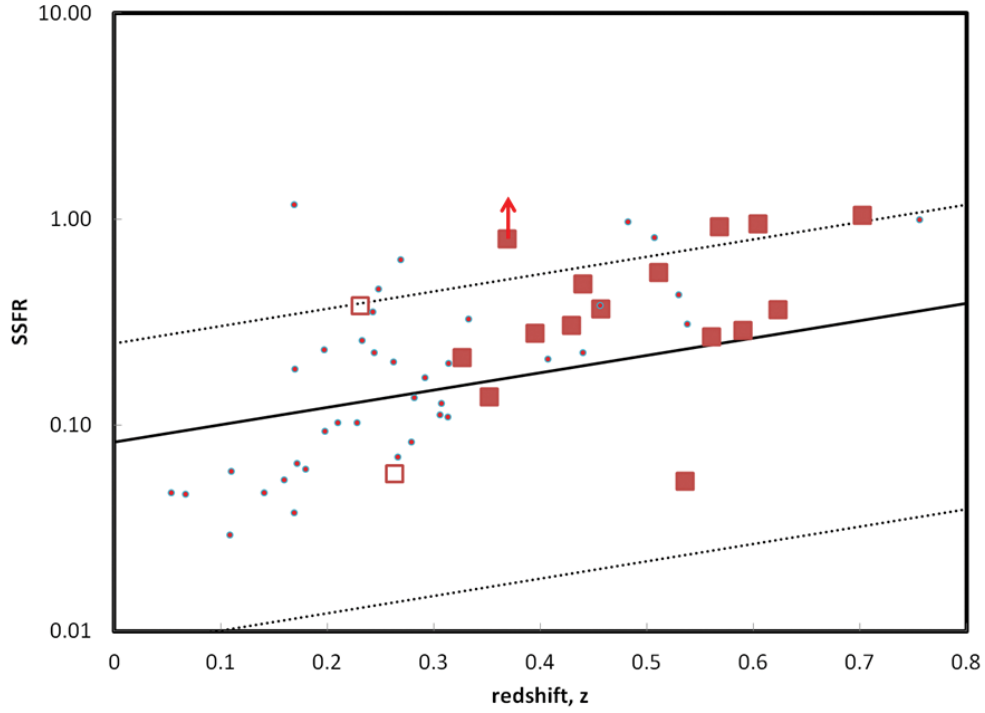


Fig. 2.— SSFR versus redshift for the *Herschel*-detected Type-2 AGNs. The solid line is the SSFR of main sequence galaxies (Elbaz, et al. 2011). The dotted lines are a factor of three times or 10% of the SSFR of main sequence galaxies, respectively. The filled boxes are for our Comparison Sample, while the unfilled boxes are the two sources with similar AGN properties but at $z < 0.3$. The small dots are for the remainder of the *Herschel*-detected type 2 galaxies. The lower limit is for J101805.93+385755.8, which is undergoing a strong starburst and for which our mass estimate is an upper limit.

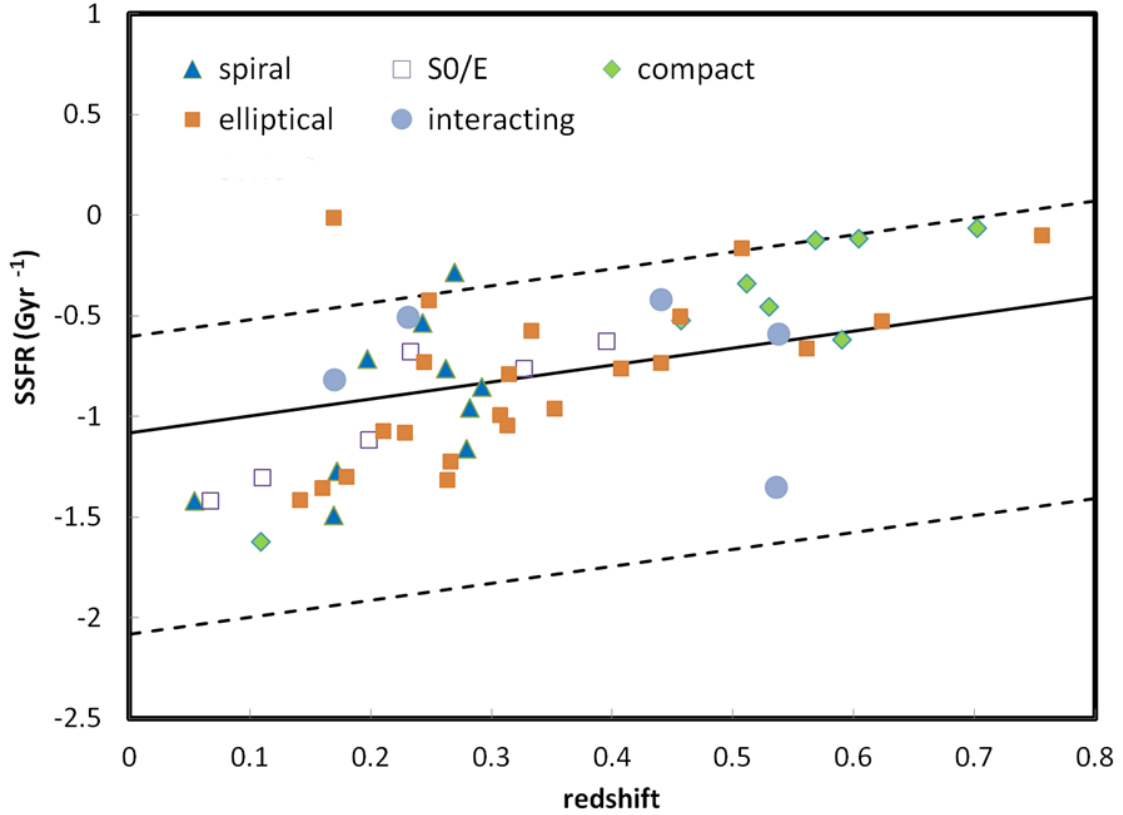


Fig. 3.— The SSFR versus redshift for *Herschel*-detected Type-2 AGNs with valid morphology classifications. The solid line is the SSFR of main sequence galaxies (Elbaz, et al. 2011). The dotted lines are a factor of three times or 10% of the SSFR of main sequence galaxies, respectively. Different symbols represent different galaxy types.

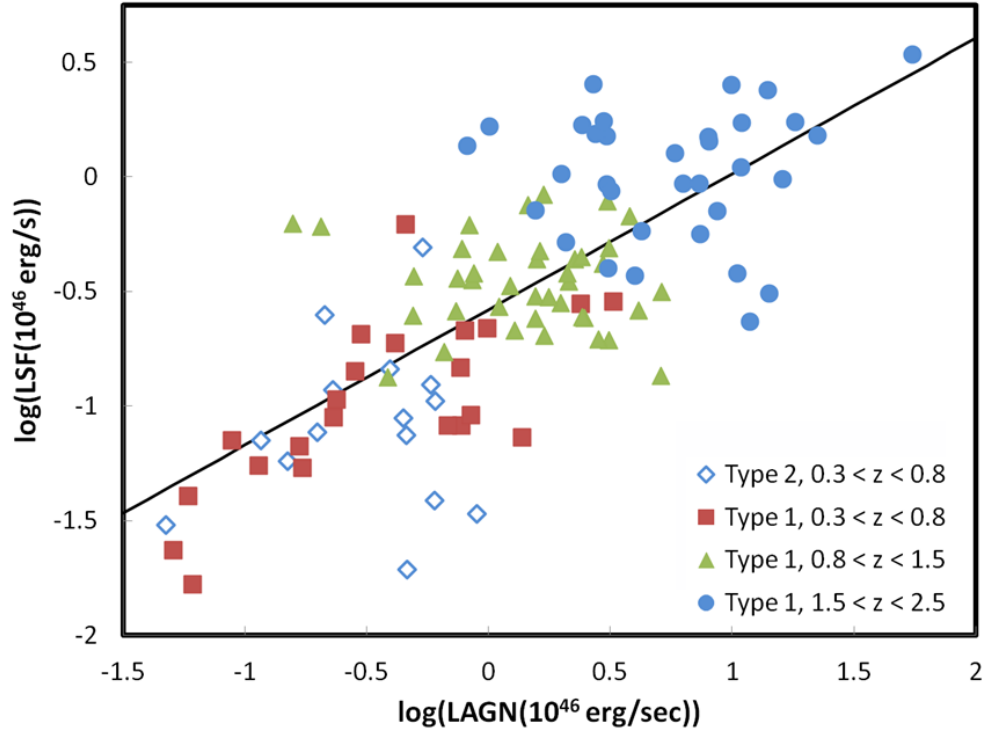


Fig. 4.— The relation between the IR luminosity of the star formation component and the AGN total luminosity. The solid line is the best-fitting unweighted relationship for all *Herschel*-detected type 1 AGN plus the Comparison Sample of type 2 AGN (selected to have nuclear properties similar to those of the type 1 sources). The fit has a slope of 0.59.

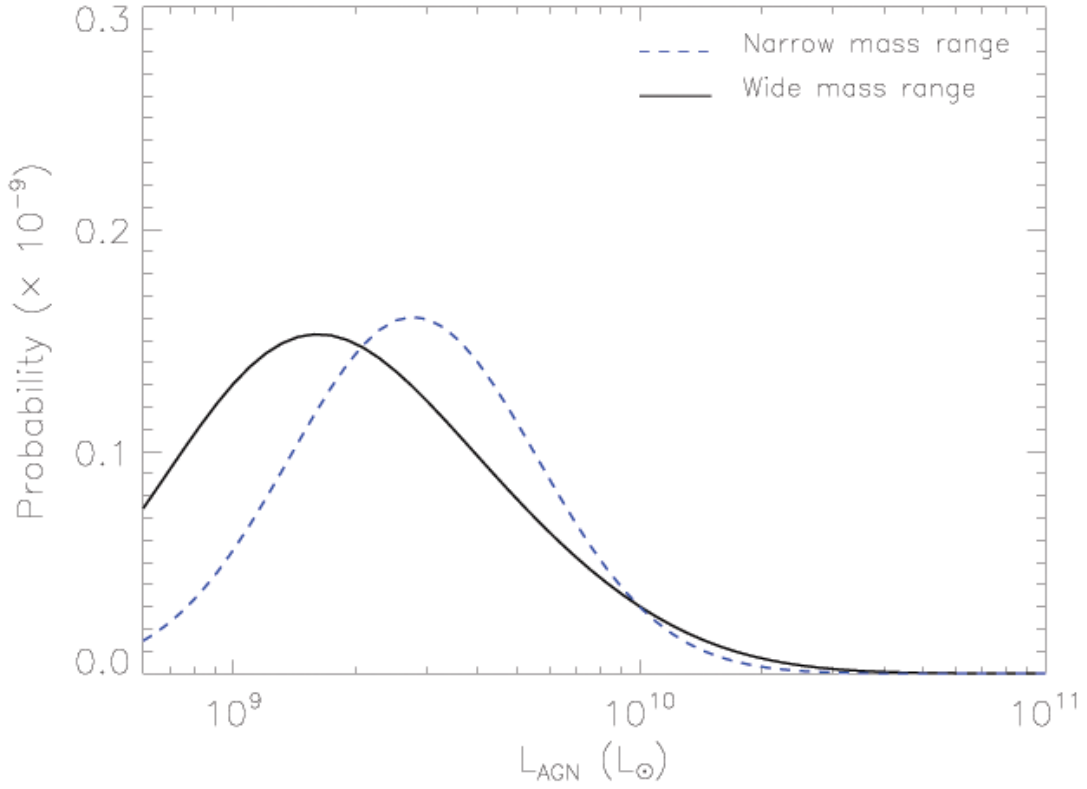


Fig. 5.— Comparison of the AGN luminosity probability distribution for two different host galaxy mass distributions. The blue dashed line represents the probability distribution for the case where the stellar masses all lie within a narrow range. The black line represents the distribution for the case where the stellar masses are spread over a range of a factor of ten. For programs that detect only a small fraction of the sample (e.g. for $L_{\text{AGN}} > 10^{10} L_{\odot}$ in this example), the detection rate can be much higher for the case where the masses are more widely spread.